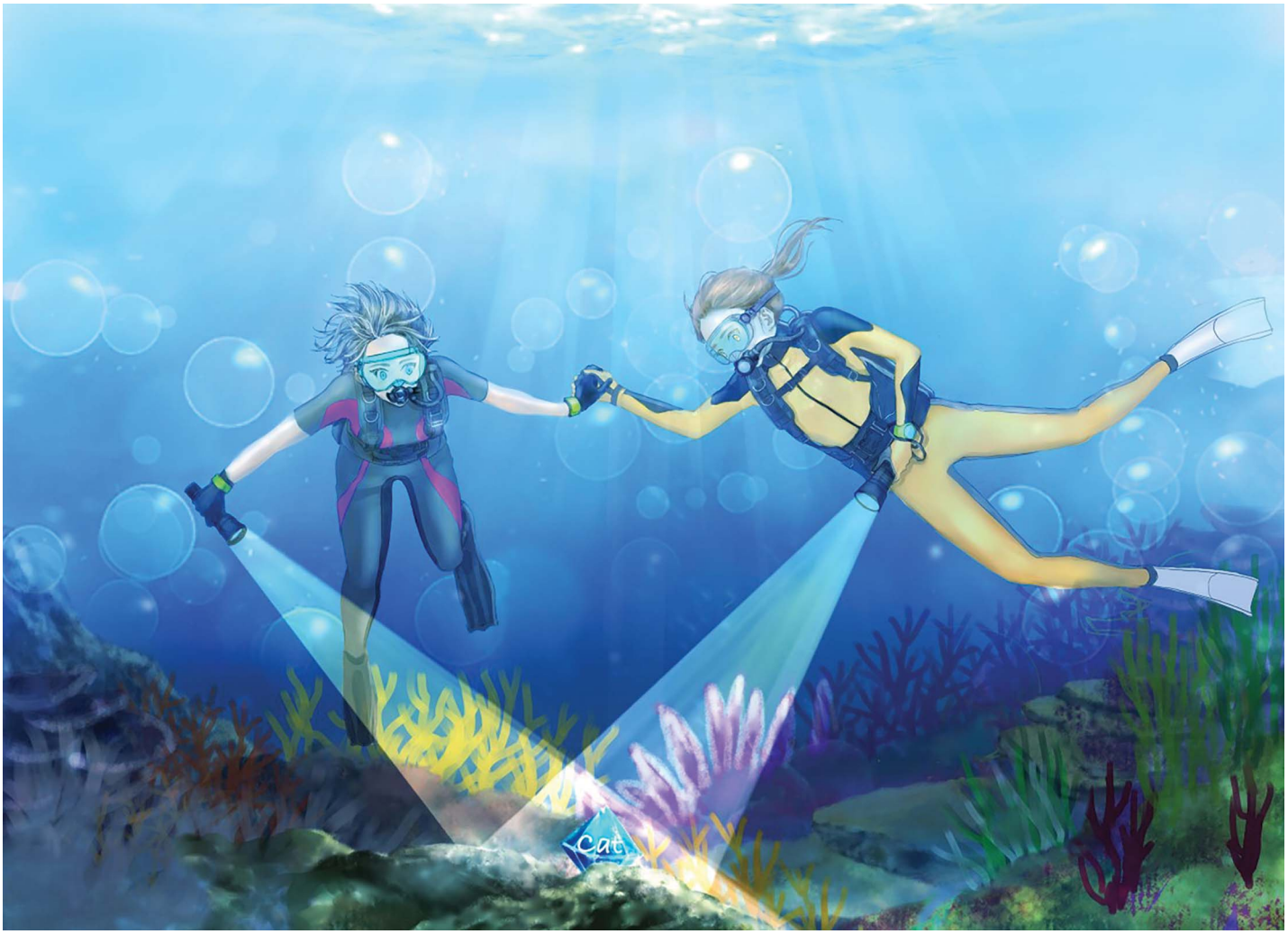

Showcasing research from the Groups of Dr. Shinji Tanaka at National Institute of Advanced Industrial Science and Technology (AIST), Japan and Professor Christophe Copéret at ETH Zürich, Switzerland. Image created by Yuko Yokoi.

DNP NMR spectroscopy enabled direct characterization of polystyrene-supported catalyst species for synthesis of glycidyl esters by transesterification

Polymer-supported catalysts have been of great interest in organic syntheses, but have suffered from the difficulty in obtaining direct structural information regarding the catalyst species embedded in the polymer due to the limitations of most analytical methods. Here, we show that dynamic nuclear polarization (DNP)-enhanced solid-state NMR is ideally positioned to characterize the ubiquitous cross-linked polystyrene (PS)-supported catalysts, thus enabling molecular-level understanding and rational development.

As featured in:

See Shinji Tanaka, Christophe Copéret *et al.*, *Chem. Sci.*, 2022, **13**, 4490.

ROYAL SOCIETY OF CHEMISTRY

rsc.li/chemical-science

Registered charity number: 207890

Chemical Science

ROYAL SOCIETY OF CHEMISTRY

EDGE ARTICLE

View Article Online
View Journal | View Issue

Cite this: *Chem. Sci.*, 2022, **13**, 4490

All publication charges for this article have been paid for by the Royal Society of Chemistry

DNP NMR spectroscopy enabled direct characterization of polystyrene-supported catalyst species for synthesis of glycidyl esters by transesterification†

Shinji Tanaka, *[ab] Yumiko Nakajima, [a] Atsuko Ogawa,[a] Takashi Kuragano,[a] Yoshihiro Kon, [a] Masanori Tamura,[a] Kazuhiko Sato[a] and Christophe Copéret *[b]

Polymer-supported catalysts have been of great interest in organic syntheses, but have suffered from the difficulty in obtaining direct structural information regarding the catalyst species embedded in the polymer due to the limitations of most analytical methods. Here, we show that dynamic nuclear polarization (DNP)-enhanced solid-state NMR is ideally positioned to characterize the ubiquitous cross-linked polystyrene (PS)-supported catalysts, thus enabling molecular-level understanding and rational development. Ammonium-based catalysts, which show excellent catalytic activity and reusability for the transesterification of methyl esters with glycidol, giving glycidyl esters in high yields, were successfully characterized by DNP ^{15}N NMR spectroscopy at ^{15}N natural abundance. DNP ^{15}N NMR shows in particular that the decomposition of quaternary alkylammonium moieties to tertiary amines was completely suppressed during the catalytic reaction. Furthermore, the dilute ring-opened product derived from glycidol and NO_3^- was directly characterized by DNP ^{15}N CPMAS and ^{1}H–^{15}N and ^{1}H–^{13}C HETCOR NMR using a ^{15}N enriched (NO_3) sample, supporting the view that the transesterification mechanism involves an alkoxide anion derived from an epoxide and NO_3^-. In addition, the detailed analysis of a used catalyst indicated that the adsorption of products on the cationic center is the major deactivation step in this catalysis.

Received 16th January 2022
Accepted 13th March 2022

DOI: 10.1039/d2sc00274d

rsc.li/chemical-science

Introduction

Immobilization of molecular catalysts on solid materials has been a strategy to intensify catalytic processes while keeping the advantages of homogeneous catalysts that are typically highly selective and more amiable to rational development.[1–4] In this context, quaternary alkyl ammonium salts are one of the most well-investigated molecular organocatalysts for base-mediated organic transformations, where a counter anion together with its ammonium cation behaves as a key reactive centre (*e.g.* phase transfer catalysis,[5] transesterification,[6–8] carbonate synthesis from CO_2 and epoxides,[9–11] *etc.*). Their immobilization has been investigated on cross-linked polystyrene (PS) because this support offers a high tolerance under basic conditions.[12–17] However, the development of PS-supported alkylammonium salt catalysts has suffered from the lack of structural characterization of the catalytic sites and how they evolve under reaction conditions.[12] For example, molecular quaternary alkylammonium salts are known to easily decompose into tertiary amines under basic conditions by Hofmann elimination and/or S_N2 substitution,[7,8] leading to significant suppression of the catalytic activity. Therefore, in order to develop highly efficient PS-supported quaternary alkylammonium salt catalysts, it is of great importance to directly trace subtle structural changes of both the cation and anion species under a PS-supported environment, although it is still a significant challenge owing to the difficulties in structural identification.

In this context, solid-state NMR has emerged as a powerful tool to characterize the local structure of solid-supported catalysts in a non-destructive manner.[18] However, its application range is often limited owing to the intrinsic low signal sensitivity of NMR. Recently, solid-state NMR enhanced by dynamic nuclear polarization (DNP) has attracted considerable attention because of its boosted signal sensitivity.[19–23] In DNP NMR, the microwave-driven polarization transfer *via* a cross-effect with a biradical combined with further polarization transfer methods (*e.g.* cross polarization) enables the enhancement of the intensity of signals from less sensitive nuclei (*e.g.* ^{13}C, ^{15}N, and ^{17}O). With this benefit, DNP NMR is nowadays recognized

[a]*Interdisciplinary Research Center for Catalytic Chemistry, National Institute of Advanced Industrial Science and Technology, Tsukuba, 305-8565, Japan. E-mail: shinji-tanaka@aist.go.jp*

[b]*Department of Chemistry and Applied Biosciences, ETH Zürich, Vladimir Prelog Weg 1-5, Zürich, 8093, Switzerland. E-mail: ccoperet@ethz.ch*

† Electronic supplementary information (ESI) available. See DOI: 10.1039/d2sc00274d

as a powerful tool for the characterization of heterogeneous catalysts and has mostly been explored for catalysts dispersed on high surface area oxide supports.[22,23] However, its application to organic polymer-supported materials is less explored, probably due to the lack of a versatile sample preparation method.[24–30] In this context, we have recently reported a rational guideline for DNP sample preparation from cross-linked PS, a prototypical insoluble synthetic polymer.[31] An appropriate choice of a DNP polarizing agent (PA) solution[32,33] can be predicted by the swelling properties of each polymer, thus facilitating the uniform distribution of the PA over the polymer network to achieve natural abundance (0.37%) ^{15}N NMR of quaternary alkylammonium salts in reasonable measurement time.

In this contribution, we have explored transesterification with glycidol (**GD**), giving glycidyl esters that are useful precursors of the epoxy resin, using solid organocatalysts based on PS-supported quaternary alkyl ammonium salts. Compared with the conventional epichlorohydrin process, this catalytic reaction is promising owing to the availability of biomass-derived feedstock (*i.e.* glycidol), thus contributing to the development of sustainable processes.[35] Taking advantage of our recently developed DNP NMR protocol, we have performed detailed structural analysis of PS-supported quaternary alkyl ammonium salts at various stages of the catalytic process. In particular, the robustness of the quaternary alkyl ammonium fragment was clearly confirmed by DNP ^{15}N NMR, consistent with the excellent activity and reusability for catalytic transesterification of methyl esters to glycidyl esters.[36,37] Furthermore, we have also tracked the evolution of the active species embedded in the PS network, thanks to DNP-enhanced 1D and 2D NMR spectroscopy.

Results and discussion

Considering that the substituents of the ammonium fragment play an important role in transesterification with molecular catalysts,[6,8] we first optimized the N-substituents of ammonium salts for transesterification of methyl esters with **GD**. Thus, **1-Cl**, **2-Cl**, **3-Cl**, and **4-Cl** were prepared by reactions of Merrifield resin with four types of alkyl amines, NMe_3, $NMe_2{}^nOct$, $NMe{}^nOct_2$, and $N{}^nOct_3$, respectively (Scheme 1). The amount of N-atoms in **1-Cl**–**4-Cl** was quantified by combustion analysis (see the ESI†). Their FT-IR spectra exhibited strong peaks assignable to C–H groups at 2800–3000 cm^{-1}, indicating the presence of alkyl groups (Fig. S1†). The conventional ^{13}C CPMAS NMR spectra of the catalysts displayed signals at 15–35 ppm, which were assigned to *n*-octyl groups (Fig. S2†). The signals due to carbon atoms attached to a nitrogen atom were observed as broad signals at 50–70 ppm. Based on these observations, it was confirmed that nitrogen-based functional groups were successfully introduced into PS.

Full identification of the structure around a nitrogen atom was achieved by using ^{15}N DNP NMR signals using our NMR protocol developed for PS samples.[31] Thus, the swelling test of PS-supported catalysts (**1-Cl**–**4-Cl**) with 1,1,2,2-tetrachloroethane (TCE) and dimethylsulfoxide (DMSO) was first conducted to predict the optimal PA solution (TEKPol/TCE or AMUPol/DMSO-d_6) for efficient DNP signal enhancement of the immobilized catalysts. **2-Cl**, **3-Cl**, and **4-Cl** were well swollen in both solvents, while DMSO was needed for **1-Cl**; hence, AMUPol/DMSO-d_6 was selected as the optimal PA solution (see the ESI, Table S1†). All measurements resulted in good sensitivity enhancement (ε_H = 35–56, Fig. S3(a)–(c)†); we could successfully identify ^{15}N signals at natural abundance for each sample after a reasonable measurement time (3–6 hours) (see the ESI†). The DNP build-up curve indicated a homogeneous distribution of PAs giving T_{DNP} values of 1.6 s (**2-Cl**), 1.4 s (**3-Cl**), and 1.6 s (**3-NO_3**) (Fig. S4†). Fig. 1 shows the selected ^{15}N CPMAS NMR spectra measured under DNP conditions at 102 K. **2-Cl** exhibited a ^{15}N signal assignable to a quaternary nitrogen atom at 57.5 ppm, while **3-Cl** displayed a signal at 62.4 ppm along with a shoulder as the result of the presence of different conformers due to the sterically large alkyl substituents.[31,34] These observations are consistent with our previous DNP ^{15}N CPMAS NMR studies on **1-Cl** (52.4 ppm) and **4-Cl** (61.8 and 59.6 ppm).[31] Overall, this clearly indicated that the quaternary alkylammonium moiety was introduced into the PS network.

We then investigated the PS-supported ammonium salt catalysts (**1-Cl**–**4-Cl**) in transesterification of methyl 4-nitrobenzoate (**5a**) with a slight excess of **GD** under azeotropic reflux conditions in hexane (Table 1). Although the catalytic activity of **1-Cl** was moderate (entry 2, 76% yield), **2-Cl**, **3-Cl** and **4-Cl** showed higher catalytic activity affording glycidyl 4-

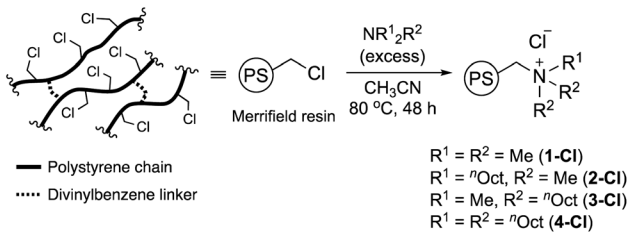

Scheme 1 Preparation of PS-supported alkylammonium catalysts **1-Cl**, **2-Cl**, **3-Cl**, and **4-Cl**.

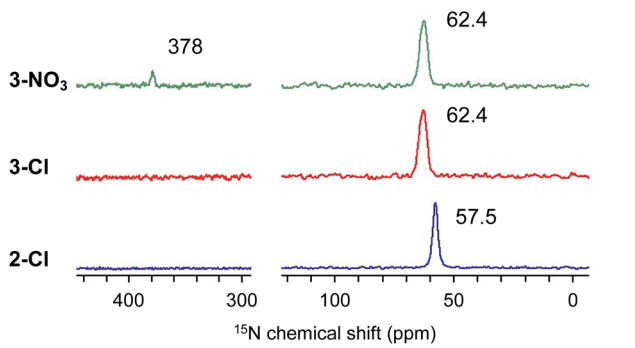

Fig. 1 DNP ^{15}N CPMAS NMR spectra of **2-Cl**, **3-Cl**, and **3-NO_3**. AMUPol/DMSO-d_6 (16 mM) was used for all measurements. MAS frequency: 10 kHz (3.2 mm rotor), CP contact time: 3 ms, recycle delay: 2.2 s (**2-Cl**), 2.0 s (**3-Cl**) and 2.1 s (**3-NO_3**), and number of scans (for ^{15}N): 7900 (**2-Cl**), 3300 (**3-Cl**), and 4096 (**3-NO_3**).

Table 1 Screening of catalysts for transesterification of methyl 4-nitrobenzoate (**5a**) with glycidol (**GD**)[a]

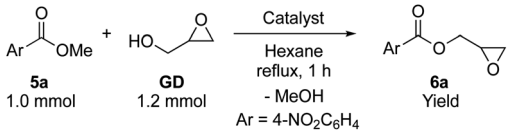

Entry	Catalyst	Loading (mol%)	Yield (%)[b]
1	None	—	3
2	**1-Cl**	5	76
3	**2-Cl**	5	94
4	**3-Cl**	5	96
5	**4-Cl**	5	92
6	**3-Cl**	0.5	90 (87)[c]

[a] Reaction conditions: a mixture of MNB (1.0 mmol), GD (1.2 mmol), and catalyst (5 mol%) in hexane (0.5 mL) was refluxed (heater temp: 80 °C) for 1 hour. [b] Yields were determined by ^{1}H NMR analysis. Values are an average of 2 runs. [c] Yield of the isolated product.

nitrobenzoate (**6a**) in 92–96% yields (entries 3–5). Of all the immobilized catalysts, **3-Cl** performed the best (entry 4, 96%). The higher activity of alkylammoniums with long-chain alkyl groups (**2-Cl**, **3-Cl** and **4-Cl**) compared to **1-Cl** parallels what is observed in homogeneous catalysis.[6] The catalytic activity of **4-Cl** was slightly lower than that of **2-Cl** and **3-Cl**, owing to the absence of the smaller Me group(s).[8] Yet, it should be noted that **1-Cl** showed lower activity in spite of the presence of three Me groups bound to nitrogen. This is probably due to the higher hydrophilicity of the polymer network in **1-Cl**, as indicated by the swelling test, which leads to the limited distribution of organic substrates.[12] **3-Cl** showed high activity even with a reduced loading of the catalyst (0.5 mol%), affording the isolated product **6a** in 87% yield (entry 6).

Table 2 Scope of the substrate for transesterification with GD using 3-Cl as a catalyst[a]

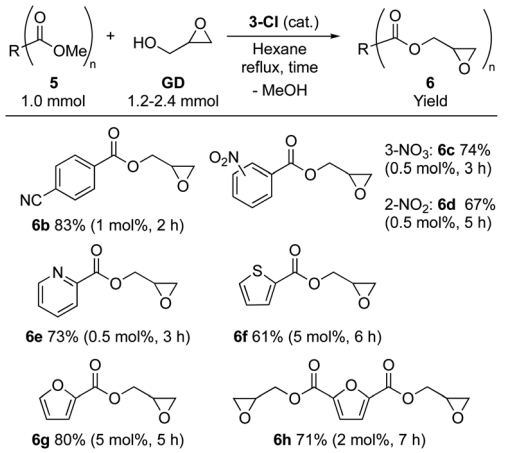

[a] Reaction conditions were optimized for each substrate. Yields of the isolated product are shown.

The substrate scope was investigated using **3-Cl** (Table 2). Glycidyl 4-cyanobenzoate (**6b**) was isolated in high yield (83%). For benzoate derivatives with a substituent at other positions (2- and 3-), glycidyl 2-nitrobenzoate (**6c**) and glycidyl 3-nitrobenzoate (**6d**) were obtained in moderate yields (**6c**: 74%, **6d**: 67%) with extended reaction time. The catalyst worked also for substrates having a heteroaromatic ring, affording glycidyl 2-pyridinecarboxylic acid (**6e**) and glycidyl 2-thiophenecarboxylic acid (**6f**) in moderate yields (**6e**: 73%, **6f**: 61%). Moreover, methyl 2-furancarboxylate (**5g**) and dimethyl 2,5-furancarboxylate (**5h**), which are useful biomass-derived substrates,[38–42] are also accessible through this approach: glycidyl esters **6g** and **6h** were isolated in good to moderate yields (**6g**: 80%, **6h**: 71%). Overall, a wide range of value-added glycidyl esters is accessible using **3-Cl**.

Next, we performed the anion exchange reaction of **3-Cl**. Our previous work revealed that weakly basic anions facilitated transesterification while suppressing self-polymerization of **GD**, which might be a major side-reaction.[43,44] Taking this result into account, we prepared **3-NO$_3$** from **3-Cl** by a sequential anion exchange *via* successive treatment with NaOH and HNO_3 (Scheme 2(a)). Since the procedure was conducted by treatment with NaOH as a strong base, one should check whether the decomposition of alkyl ammoniums possibly proceeds during the anion exchange *via* S_N2 substitution (paths A and B_1) and/or Hofmann elimination (path B_2) which results in the formation of tertiary amine moieties (Scheme 2(b)). To confirm this point, we performed DNP ^{15}N NMR analysis to monitor ^{15}N signals before and after the anion exchange reaction. As clearly shown from the DNP ^{15}N NMR spectrum of **3-NO$_3$**, no additional signals except for NO_3^- at 378 ppm were observed after the anion exchange (Fig. 1). Furthermore, PS-supported tertiary amines **7** and **8** were alternatively synthesized by the reaction of Merrifield resin with secondary amines (see the ESI†). DNP ^{15}N NMR spectra of **7** and **8** exhibited signals at 25–60 ppm, which appeared as broad signals presumably due to the existence of distinct conformers at cryogenic temperature due to the bulky tertiary amines[45] (see the ESI, Fig. S5†). As a result, we confirmed that the quaternary ammonium fragment was maintained after the anion exchange procedure.

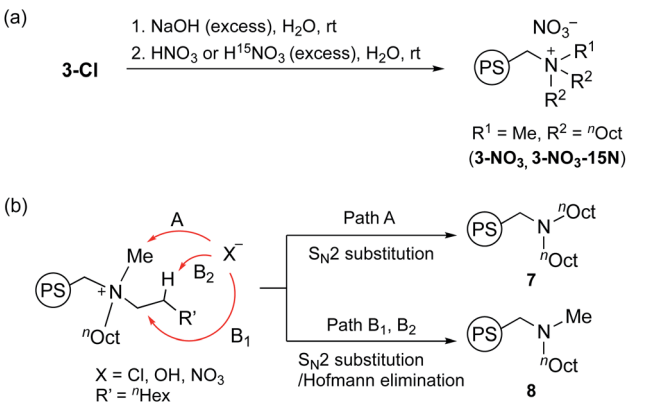

Scheme 2 Anion exchange reaction of 3-Cl to 3-NO$_3$ and 3-NO$_3$-^{15}N (a), and possible decomposition pathways of quaternary alkylammonium moieties to tertiary amines **7** and **8** (b).

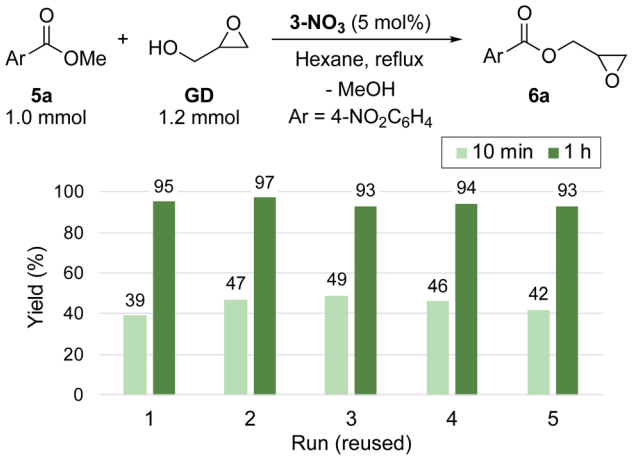

Scheme 3 Reuse test of **3-NO$_3$** toward the synthesis of **2a**.

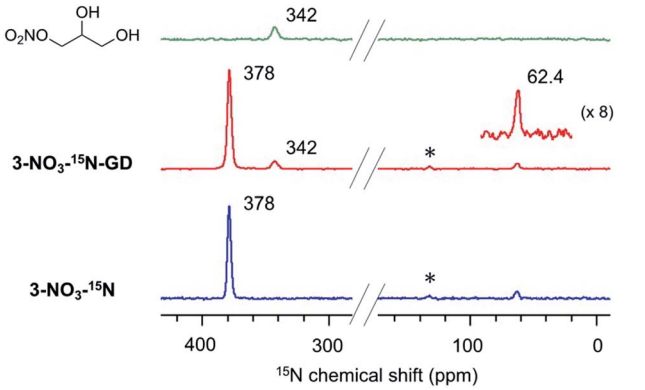

Fig. 2 DNP ^{15}N CPMAS NMR spectra of 1-nitro-2,3-propanediol (top), **3-NO$_3$-^{15}N-GD** (middle) and **3-NO$_3$-^{15}N** (bottom). AMUPol/DMSO-d$_6$ (16 mM) was used as a PA. MAS frequency: 10 kHz (3.2 mm rotor), CP contact time: 3 ms (1-nitro-2,3-propanediol) and 8 ms (**3-NO$_3$-^{15}N-GD**, **3-NO$_3$-^{15}N**), recycle delay: 3.3 s (1-nitro-2,3-propanediol), 2.1 s (**3-NO$_3$-^{15}N-GD**), and 2.5 s (**3-NO$_3$-^{15}N**), and number of scans: 128 (a), 512 (b), 2048 (**3-NO$_3$-^{15}N-GD**), and 1024 (**3-NO$_3$-^{15}N**). Peaks with an asterisk are spinning side-band signals.

3-NO$_3$ exhibited comparable high catalytic activity with **3-Cl** towards transesterification (Scheme 3), enabling the efficient synthesis of glycidyl esters in a chlorine-free manner, which is crucial for the production of high-grade epoxy resins utilized for insulating materials.[36] With this catalyst in hand, we further performed a reuse test for catalytic transesterification. Reusability is one of the key advantages of supported catalysts, generally relying on the stability of the catalyst under the reaction conditions. In this system, as described above, the decomposition of quaternary ammonium moieties into tertiary amines is a major pathway for catalyst deactivation (Scheme 2(b)). To reveal the catalytic behaviour of **3-NO$_3$**, we performed the reuse test with 5 mol% loading with a short reaction time (10 min). Under these conditions, **3-NO$_3$** catalysed the transesterification of **5a** with **GD** to give **6a** in 39% yield in the first run. Interestingly, the activity was slightly improved in the second run (47%), and only slightly decreased after further reuse (5th: 42%) (Scheme 3). This result indicates that only a small structural transformation happened at the catalytically active site in PS. We note that the yield of **6a** was excellent even in the fifth run under conditions with an extended reaction time (1 h), confirming the significant utility of this catalyst for the synthesis of glycidyl esters (Scheme 3).

The peculiar catalytic behaviour in the recycling study prompted us to gain insights into the active species on PS in a direct manner using DNP NMR. Our previous experimental and computational studies have implied that the ring-opening of glycidol affords the active anion that initiates transesterification by abstracting a proton from the substrate alcohol.[6] It is also reported that the ring-opened species from epoxides and weak anions behave as an intermediate for the catalytic cycle of cyclic carbonate and polycarbonate synthesis from epoxides and CO_2.[9–11] Because a high concentration of ring-opened species leads to the self-oligomerization of the epoxide, a dilute condition is necessary for achieving high yields of the product, yet such dilute species are not observable by conventional analytical methods. For an in-depth study of such dilute ring-opened species by DNP NMR spectroscopy,[46] we prepared **3-NO$_3$-^{15}N** using ^{15}N-enriched HNO_3. Moreover, the sample **3-NO$_3$-^{15}N-GD** was synthesized by the reaction of **3-NO$_3$-^{15}N** with 2 equiv. of **GD** in hexane (see the ESI†). The DNP ^{15}N CPMAS NMR spectrum of **3-NO$_3$-^{15}N-GD** with AMUPol/DMSO-d$_6$ displayed an additional signal at 342 ppm along with the original signals of **3-NO$_3$-^{15}N** (62.4 and 378 ppm) (Fig. 2). To identify the product that exhibits the signal at 342 ppm, we prepared 1-nitro-2,3-propanediol as a possible ring-opened compound derived from **GD** and NO_3^-.[47] As expected, the DNP ^{15}N CPMAS NMR spectrum of 1-nitro-2,3-propanediol under the same conditions (AMUPol/DMSO-d$_6$) also showed a ^{15}N signal at 342 ppm (Fig. 2). Thus, it was possible to prove that the ring-opened product 1-nitro-2,3-propanediol was formed during catalysis. For further characterization of ring-opened species, we performed DNP-enhanced ^{1}H–^{15}N and ^{1}H–^{13}C HETCOR NMR of **3-NO$_3$-^{15}N-GD**. The ^{1}H–^{15}N HETCOR spectrum showed a correlation peak between the ^{15}N signal at 342 ppm and the ^{1}H signal at 4.1 ppm (Fig. 3(a)). In addition, the ^{13}C signal at 73 ppm, which newly appeared after conversion of glycidol to **3-NO$_3$-^{15}N**, was also correlated with the ^{1}H signal at 4.1 ppm in the ^{1}H–^{13}C HETCOR spectrum (Fig. 3(b)). These observations strongly supported the presence of a ring-opened product bearing NO_3 at the terminal position (δ_C ~76 ppm) of **GD** rather than at an internal position (δ_C ~86 ppm).[47] This result is consistent with the general regio-selectivity of ring-opening of epoxides under basic conditions. Because the signal of the ring-opened product was not significantly correlated with either alkyl (1.2 ppm for ^{1}H) or aromatic groups (7.0 ppm for ^{1}H) under these conditions (CP contact time: 1 ms (^{15}N), 0.2 ms (^{13}C)), the ring-opened product likely exists in a protonated form,[48] which is free from a cationic moiety in PS. Because decomposition of the quaternary ammonium fragment to a tertiary amine was not observed (Fig. 2), another **GD** molecule presumably worked as a proton source, generating a deprotonated **GD** (Scheme 4). As transesterification proceeds *via* an attack of the deprotonated **GD** on the carbonyl moiety of

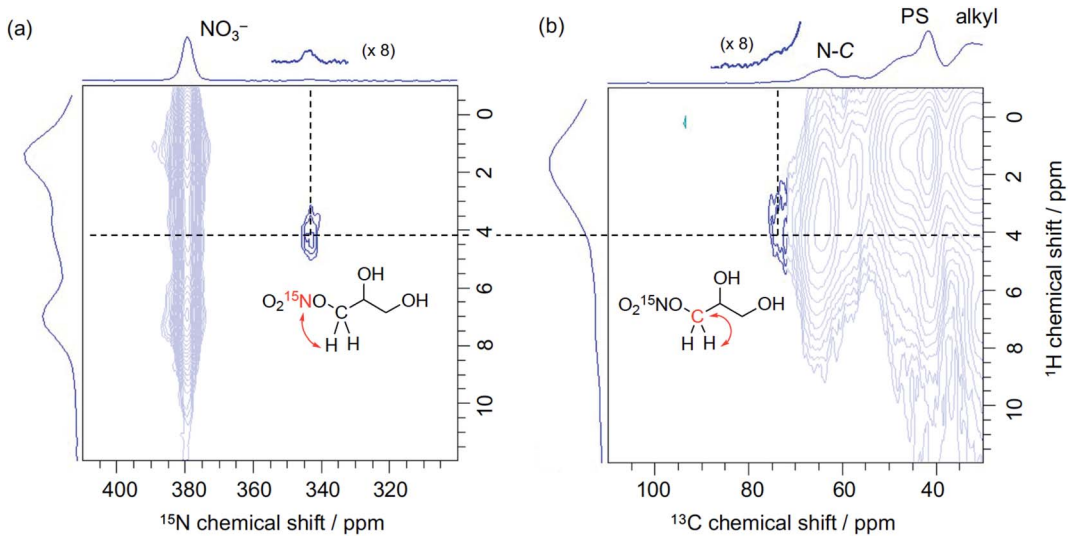

Fig. 3 DNP ^{1}H–^{15}N HETCOR (a) and DNP ^{1}H–^{13}C HETCOR spectra (b) of **3-NO$_3$-^{15}N-GD**. AMUPol/DMSO-d$_6$ (16 mM) was used as a PA. FSLG (frequency-switched Lee-Goldburg) homonuclear decoupling was employed during the evolution of the ^{1}H chemical shift. A decoupling field of 100 kHz was used. MAS frequency: 10 kHz (3.2 mm rotor for ^{15}N and 1.9 mm rotor for ^{13}C), CP contact time: 1 ms (for ^{15}N) and 0.2 ms (for ^{13}C), recycle delay: 2 s (for ^{15}N) and 2.5 s (for ^{13}C) and number of scans: 32 (for ^{15}N) and 64 (for ^{13}C).

the ester, the presented results clearly support the mechanism that involves *in situ* generated active anion species. Overall, the observations by DNP NMR successfully evidenced the formation of ring-opened species derived from epoxides in an initiation step of the catalytic transesterification. The consumption of **GD** for the generation of active species likely explains the slightly lower product yield in the first run in the catalyst reuse test (Scheme 3).

Next, our aim was to understand the deactivation step. To shed light on the deactivated species for this PS-immobilized material, we analysed the catalyst moieties embedded in PS after the catalytic reaction. The DNP ^{15}N CPMAS NMR spectrum of **3-NO$_3$** following five catalytic runs indicated that the signal of the quaternary ammonium fragment at 62.4 ppm remained unchanged, while no signal associated with tertiary amines was present. This confirms that the quaternary ammonium fragment remains intact even after five runs (Fig. 4(a)). Interestingly, a signal centered at 370 ppm was newly observed and was assigned to the nitro group (NO_2). The DNP ^{13}C CPMAS NMR spectrum showed signal(s) from the ester group at 158 ppm and broad shoulder signals due to a ring-opened epoxide moiety at 60–75 ppm (Fig. 4(b)). Consequently, it is likely that ring-opened

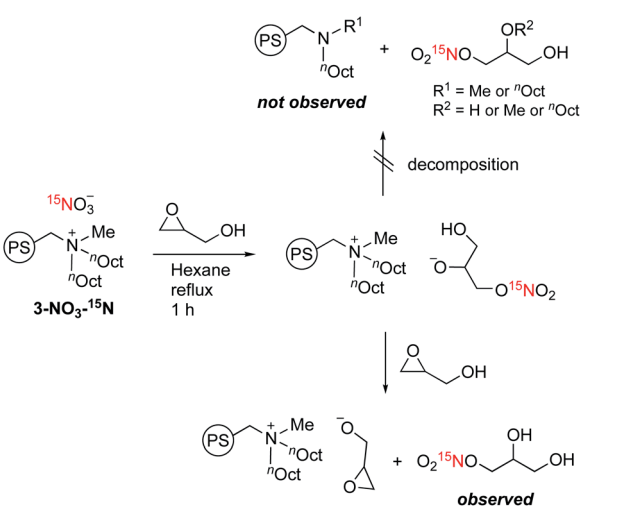

Scheme 4 Plausible mechanism of generation of ring-opened species from an epoxide and an NO_3 anion and the reaction with proton sources.

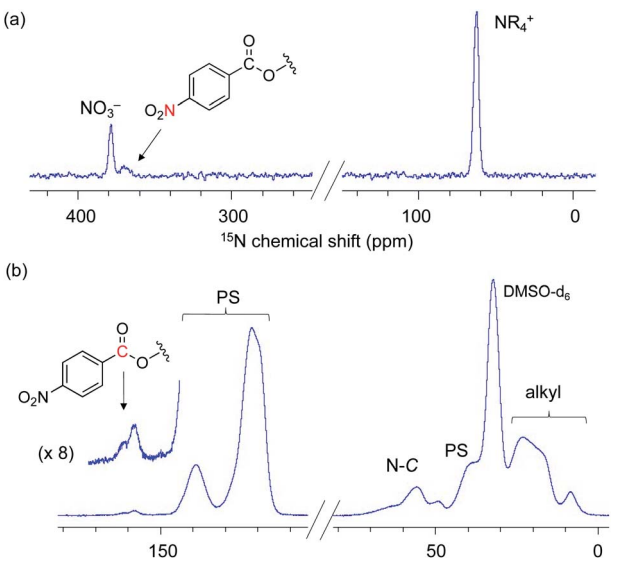

Fig. 4 DNP ^{15}N CPMAS NMR (a) and DNP ^{13}C CPMAS NMR spectra (b) of **3-NO$_3$** after five reuse cycles for the catalytic reaction. AMUPol/DMSO-d$_6$ (16 mM) was used as a PA. MAS frequency: 10 kHz (3.2 mm rotor), CP contact time: 3 ms, recycle delay: 4.4 s, and number of scans: 6000 (a) and 512 (b).

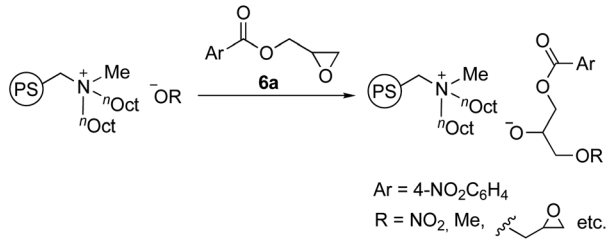

Scheme 5 Formation of ring-opened species derived from the product.

species derived from **6a** or its oligomerized forms are adsorbed during catalysis (Scheme 5). In other words, the major deactivation step of this catalysis is not the decomposition of the quaternary alkyl ammonium moiety itself, but is likely associated with the adsorption of products on a cationic moiety, inhibiting efficient catalyst turnover. This observation explains the slight loss of catalytic activity after several runs (Scheme 3). Understanding of the unusual deactivation mechanism of the alkylammonium salt catalyst, which was enabled with the help of DNP NMR spectroscopy, is certainly helpful toward the rational improvement of the catalyst.

Conclusions

In conclusion, we developed a well-defined PS-supported alkylammonium salt catalyst, which showed excellent catalytic activity and reusability for transesterification of methyl esters with **GD**, giving glycidyl esters in high yields. We also demonstrated that DNP NMR is a reliable analytical method to characterize and monitor the stability of PS-supported alkylammonium salt catalysts without the need for labelling strategies. The stability of the alkylammonium moiety, which is known to decompose into the inactive tertiary amine, was successfully monitored by DNP ^{15}N NMR: the absence of formation of tertiary amines in these supported catalysts under the mild basic conditions used in this study is consistent with their very good stability and reusability. DNP NMR also helped us to obtain a mechanistic insight into the generation of reaction intermediates and active species. Furthermore, a ring-opened product derived from **GD** and NO_3^- was directly characterized by DNP ^{15}N CPMAS and ^{1}H–^{15}N and ^{1}H–^{13}C HETCOR NMR using a ^{15}N enriched (NO_3) sample. The direct characterization of the used catalyst allowed us to gain a new insight into the deactivation mechanism, which is helpful for the rational improvement of catalysts. This study showcases how DNP NMR spectroscopy can provide unique molecular-level information regarding the active sites of polymer-supported catalysts. Further application of DNP NMR to various polymer-supported catalysts as well as high-performance polymer materials is ongoing in our laboratory.

Data availability

All available data are included in ESI.†

Author contributions

S. T.: conceptualization, investigation (NMR measurements), and writing – original draft. Y. N.: writing – review & editing. A. O. and T. K.: investigation (synthesis and catalysis). Y. K. and M. T.: supervision. K. S.: project administration and supervision. C. C.: conceptualization and writing – review & editing. All the authors have given approval to the final version of the manuscript.

Conflicts of interest

There are no conflicts to declare.

Acknowledgements

This work was partially funded by the New Energy and Industrial Technology Development Organization of Japan (NEDO) (Grant JPNP16010). Dr S. Tanaka acknowledges financial support by a Grant-in-Aid for Early-Career Scientists (JSPS KAKENHI Grant Number JP20K15329). Prof. C. Copéret is thankful for the JSPS program that allowed many discussions regarding the presented research. We acknowledge Mr Takuya Nakashima for preliminary studies on PS-supported catalysts.

Notes and references

1 M. R. Buchmeiser, Polymer-Supported Well-Defined Metathesis Catalysts, *Chem. Rev.*, 2009, **109**, 303–321.
2 M. P. Conley, C. Copéret and C. Thieuleux, Mesostructured Hybrid Organic–Silica Materials: Ideal Supports for Well-Defined Heterogeneous Organometallic Catalysts, *ACS Catal.*, 2014, **4**, 1458–1469.
3 R. Zhong, A. C. Lindhorst, F. J. Groche and F. E. Kühn, Immobilization of *N*-Heterocyclic Carbene Compounds: A Synthetic Perspective, *Chem. Rev.*, 2017, **117**, 1970–2058.
4 W. Wang, L. Cui, P. Sun, L. Shi, C. Yue and F. Li, Reusable N-Heterocyclic Carbene Complex Catalysts and Beyond: A Perspective on Recycling Strategies, *Chem. Rev.*, 2018, **118**, 9843–9929.
5 *Asymmetric Phase Transfer Catalysis*, ed. K. Maruoka, Wiley-VCH, Weinheim, 2008.
6 S. Tanaka, T. Nakashima, T. Maeda, M. Ratanasak, J. Hasegawa, Y. Kon, M. Tamura and K. Sato, Quaternary Alkyl Ammonium Salt-Catalyzed Transformation of Glycidol to Glycidyl Esters by Transesterification of Methyl Esters, *ACS Catal.*, 2018, **8**, 1097–1103.
7 S. Tanaka, T. Nakashima, N. Satou, H. Oono, Y. Kon, M. Tamura and K. Sato, Epoxide as precatalyst for metal-free catalytic transesterification, *Tetrahedron Lett.*, 2019, **60**, 2009–2013.
8 M. Hatano, Y. Tabata, Y. Yoshida, K. Toh, K. Yamashita, Y. Ogura and K. Ishihara, Metal-free transesterification catalyzed by tetramethylammonium methyl carbonate, *Green Chem.*, 2018, **20**, 1193–1198.
9 V. Caló, A. Nacci, A. Monopoli and A. Fanizzi, Cyclic Carbonate Formation from Carbon Dioxide and Oxiranes

in Tetrabutylammonium Halides as Solvents and Catalysts, *Org. Lett.*, 2002, **4**, 2561–2563.

10 Y. Xie, Z. Zhang, T. Jiang, J. He, B. Han, T. Wu and K. Ding, CO_2 Cycloaddition Reactions Catalyzed by an Ionic Liquid Grafted onto a Highly Cross-Linked Polymer Matrix, *Angew. Chem., Int. Ed.*, 2007, **46**, 7255–7258.

11 F. Della Monica, A. Buonerba, A. Grassi, C. Capacchione and S. Milione, Glycidol: an Hydroxyl-Containing Epoxide Playing the Double Role of Substrate and Catalyst for CO_2 Cycloaddition Reactions, *ChemSusChem*, 2016, **9**, 3457–3464.

12 D. C. Sherrington, Preparation, structure and morphology of polymer supports, *Chem. Commun.*, 1998, 2275–2286.

13 A. R. Vaino and K. D. Janda, Solid-Phase Organic Synthesis: A Critical Understanding of the Resin, *J. Comb. Chem.*, 2000, **2**, 579–596.

14 J. Lu and P. H. Toy, Organic Polymer Supports for Synthesis and for Reagent and Catalyst Immobilization, *Chem. Rev.*, 2009, **109**, 815–838.

15 C. A. McNamara, M. J. Dixon and M. Bradley, Recoverable Catalysts and Reagents Using Recyclable Polystyrene-Based Supports, *Chem. Rev.*, 2002, **102**, 3275–3300.

16 S. Itsuno and M. M. Hassan, Polymer-immobilized chiral catalysts, *RSC Adv.*, 2014, **4**, 52023–52043.

17 B. Altava, M. I. Burguete, E. García-Verdugo and S. V. Luis, Chiral catalysts immobilized on achiral polymers: effect of the polymer support on the performance of the catalyst, *Chem. Soc. Rev.*, 2018, **47**, 2722–2771.

18 M. R. Hansen, R. Graf and H. W. Spiess, Interplay of Structure and Dynamics in Functional Macromolecular and Supramolecular Systems As Revealed by Magnetic Resonance Spectroscopy, *Chem. Rev.*, 2015, **116**, 1272–1308.

19 *Handbook of High-Field Dynamic Nuclear Polarization*, ed. V. K. Michaelis, R. G. Griffin, B. Corzilius, and S. Vega, John Wiley & Sons, 2020.

20 Y. C. Su, L. Andreas and R. G. Griffin, Magic Angle Spinning NMR of Proteins: High-Frequency Dynamic Nuclear Polarization and H-1 Detection, *Annu. Rev. Biochem.*, 2015, **84**, 465–497.

21 A. J. Rossini, Materials Characterization by Dynamic Nuclear Polarization-Enhanced Solid-State NMR Spectroscopy, *J. Phys. Chem. Lett.*, 2018, **9**, 5150–5159.

22 T. Kobayashi, F. A. Perras, I. I. Slowing, A. D. Sadow and M. Pruski, Dynamic Nuclear Polarization Solid-State NMR in Heterogeneous Catalysis Research, *ACS Catal.*, 2015, **5**, 7055–7062.

23 W.-C. Liao, B. Ghaffari, C. P. Gordon, J. Xu and C. Copéret, Dynamic Nuclear Polarization Surface Enhanced NMR Spectroscopy (DNP SENS): Principles, Protocols, and Practice, *Curr. Opin. Colloid Interface Sci.*, 2018, **33**, 63–71.

24 D. Le, G. Casano, T. N. T. Phan, F. Ziarelli, O. Ouari, F. Aussenac, P. Thureau, G. Mollica, D. Gigmes, P. Tordo and S. Viel, Optimizing Sample Preparation Methods for Dynamic Nuclear Polarization Solid-state NMR of Synthetic Polymers, *Macromolecules*, 2014, **47**, 3909–3916.

25 O. Ouari, T. Phan, F. Ziarelli, G. Casano, F. Aussenac, P. Thureau, D. Gigmes, P. Tordo and S. Viel, Improved Structural Elucidation of Synthetic Polymers by Dynamic Nuclear Polarization Solid-State NMR Spectroscopy, *ACS Macro Lett.*, 2013, **2**, 715–719.

26 G. N. Manjunatha Reddy, J. A. Gerbec, F. Shimizu and B. F. Chmelka, Nanoscale Surface Compositions and Structures Influence Boron Adsorption Properties of Anion Exchange Resins, *Langmuir*, 2019, **35**, 15661–15673.

27 F. Blanc, S. Y. Chong, T. O. McDonald, D. J. Adams, S. Pawsey, M. A. Caporini and A. I. Cooper, Dynamic Nuclear Polarization NMR Spectroscopy Allows High-Throughput Characterization of Microporous Organic Polymers, *J. Am. Chem. Soc.*, 2013, **135**, 15290–15293.

28 N. J. Brownbill, R. S. Sprick, B. Bonillo, S. Pawsey, F. Aussenac, A. J. Fielding, A. I. Cooper and F. Blanc, Structural Elucidation of Amorphous Photocatalytic Polymers from Dynamic Nuclear Polarization Enhanced Solid State NMR, *Macromolecules*, 2018, **51**, 3088–3096.

29 S. Grätz, M. de Olivera Junior, T. Gutmann and L. Borchardt, A comprehensive approach for the characterization of porous polymers using 13C and 15N dynamic nuclear polarization NMR spectroscopy, *Phys. Chem. Chem. Phys.*, 2020, **22**, 23307–23314.

30 T. Kanda, M. Kitawaki, T. Arata, Y. Matsuki and T. Fujiwara, Structural analysis of cross-linked poly(vinyl alcohol) using high-field DNP-NMR, *RSC Adv.*, 2020, **10**, 8039–8043.

31 S. Tanaka, W.-C. Liao, A. Ogawa, K. Sato and C. Copéret, DNP NMR spectroscopy of cross-linked organic polymers: rational guidelines towards optimal sample preparation, *Phys. Chem. Chem. Phys.*, 2020, **22**, 3184–3190.

32 A. Zagdoun, G. Casano, O. Ouari, M. Schwarzwalder, A. J. Rossini, F. Aussenac, M. Yulikov, G. Jeschke, C. Coperet, A. Lesage, P. Tordo and L. Emsley, Large Molecular Weight Nitroxide Biradicals Providing Efficient Dynamic Nuclear Polarization at Temperatures up to 200 K, *J. Am. Chem. Soc.*, 2013, **135**, 12790–12797.

33 C. Sauvée, M. Rosay, G. Casano, F. Aussenac, R. T. Weber, O. Ouari and P. Tordo, Highly Efficient, Water-Soluble Polarizing Agents for Dynamic Nuclear Polarization at High Frequency, *Angew. Chem., Int. Ed.*, 2013, **52**, 10858–10861.

34 V. B. Luzhkov, F. Österberg, P. Acharya, J. Chattopadhyaya and J. Åqvist, Computational and NMR study of quaternary ammonium ion conformations in solution, *Phys. Chem. Chem. Phys.*, 2002, **4**, 4640–4647.

35 D. Cespi, R. Cucciniello, M. Ricciardi, C. Capacchione, I. Vassura, F. Passarini and A. Proto, A simplified early stage assessment of process intensification: glycidol as a value-added product from epichlorohydrin industry wastes, *Green Chem.*, 2016, **18**, 4559–4570.

36 J. P. Pascault, and R. J. Williams, In *Epoxy Polymers: New Materials and Innovations*, ed.Pascault, J. P. and Williams, R. J. J., Wiley-VCH, Weinheim, Germany, 2010, pp. 1–12.

37 S. Zhang, T. Liu, C. Hao, A. Mikkelsen, B. Zhao and J. Zhang, Hempseed Oil-Based Covalent Adaptable Epoxy-Amine Network and Its Potential Use for Room-Temperature Curable Coatings, *ACS Sustainable Chem. Eng.*, 2020, **8**, 14964–14974.

38 L. Zhang, X. Luo, Y. Qin and Y. Li, A novel 2,5-furandicarboxylic acid-based bis(cyclic carbonate) for the synthesis of biobased non-isocyanate polyurethanes, *RSC Adv.*, 2017, **7**, 37–46.

39 A. Marotta, V. Ambrogi, P. Cerruti and A. Mija, Green approaches in the synthesis of furan-based diepoxy monomers, *RSC Adv.*, 2018, **8**, 16330–16335.

40 S. Nameer, D. B. Larsen, J. Ø. Duus, A. E. Daugaard and M. Johansson, Biobased Cationically Polymerizable Epoxy Thermosets from Furan and Fatty Acid Derivatives, *ACS Sustainable Chem. Eng.*, 2018, **6**, 9442–9450.

41 J. Meng, Y. Zeng, P. Chen, J. Zhang, C. Yao, Z. Fang and K. Guo, New ultrastiff bio-furan epoxy networks with high Tg: Facile synthesis to excellent properties, *Eur. Polym. J.*, 2019, **121**, 109292.

42 G. Wang, L. Lopez, M. Coile, Y. Chen, J. M. Torkelson and L. J. Broadbelt, Identification of Known and Novel Monomers for Poly(hydroxyurethanes) from Biobased Materials, *Ind. Eng. Chem. Res.*, 2021, **60**, 6814–6825.

43 D. Wilms, S.-E. Stiriba and H. Frey, *Acc. Chem. Res.*, 2010, **43**, 129–141.

44 R. Haag, A. Sunder and J.-F. Stumbe, *J. Am. Chem. Soc.*, 2000, **122**, 2954–2955.

45 C. H. Bushweller, S. H. Fleischman, G. L. Grady, P. McGoff, C. D. Rithner, M. R. Whalon, J. G. Brennan, R. P. Marcantonio and R. P. Dominigue, Stereodynamics of diethylmethylamine and triethylamine, *J. Am. Chem. Soc.*, 1982, **104**, 6224–6236.

46 F. Ziarelli, M. Casciola, M. Pica, A. Donnadio, F. Aussenac, C. Sauvee, D. Capitani and S. Viel, Dynamic nuclear polarisation NMR of nanosized zirconium phosphate polymer fillers, *Chem. Commun.*, 2014, **50**, 10137–10139.

47 K. Lange, A. Koenig, C. Roegler, A. Seeling and J. Lehmann, NO donors. Part 18: Bioactive metabolites of GTN and PETN—Synthesis and vasorelaxant properties, *Bioorg. Med. Chem. Lett.*, 2009, **19**, 3141–3144.

48 A. Leal-Duaso, M. Caballero, A. Urriolabeitia, J. A. Mayoral, J. I. García and E. Pires, Synthesis of 3-alkoxypropan-1,2-diols from glycidol: experimental and theoretical studies for the optimization of the synthesis of glycerol derived solvents, *Green Chem.*, 2017, **19**, 4176–4185.